

Transport properties of one-dimensional Kronig-Penney models with correlated disorder

Tsampikos Kottos¹, G. P. Tsironis¹ and Felix M. Izrailev^{1,2*}

¹ Department of Physics, University of Crete
and Research Center of Crete, P.O. Box 1527
71110 Heraklion-Crete, Greece

² Budker Institute of Nuclear Physics, Novosibirsk 630090, Russia

September 17, 2021

Abstract

Transport properties of one-dimensional Kronig-Penney models with binary correlated disorder are analyzed using an approach based on classical Hamiltonian maps. In this method, extended states correspond to bound trajectories in the phase space of a parametrically excited linear oscillator, while the on site-potential of the original model is transformed to an external force. We show that in this representation the two probe conductance takes a simple geometrical form in terms of evolution areas in phase-space. We also analyze the case of a general N -mer model.

*email addresses: izrailev@vxinp.inp.nsk.su ; izrailev@physics.spa.umn.edu

1 Introduction

The random dimer model, a tight binding model with correlated disorder, introduced in refs. [1, 2] has attracted considerable attention due to the presence of transparent states in an otherwise disordered one dimensional system [1]-[9]. In the present paper we address the issue of the spectrum of the random dimer Kronig-Penney (RDKP) model [10] and extensions using the same Hamiltonian approach applied earlier in the context of the tight binding models [9]. Using techniques from dynamical systems theory [11], we construct a Poincare map that turns the Kronig-Penney model into an equivalent tight-binding model and study the latter through a two-dimensional map corresponding to a classical linear oscillator with a parametric perturbation given in the form of periodic delta-kicks [9]. The amplitudes of these kicks are defined by the site potential of the tight-binding model. In this representation, extended states of the tight-binding model are represented through bounded trajectories in the phase space of the Hamiltonian map. Furthermore, in this representation the two probe conductance is related to the time evolution (under the Hamiltonian map) of areas initially defined by the basis unit vectors. This new approach provides an effective and simple tool for understanding transport properties, the structure of eigenstates as well as for deriving analytical expressions. In particular, one can easily determine fully transparent states for the general case when N -sites are correlated. In the following section we summarize briefly the Hamiltonian map approach used in ref. [9] and apply it in the context of the RDKP model. In section 3 we analyze transport properties through a new expression for conductance while in section 4 we conclude.

2 Hamiltonian Map Approach

2.1 Time-Dependent Linear Map

The model of interest is the one-dimensional Schrödinger equation with an array of δ -function potentials:

$$E\phi(z) = -\frac{d^2\phi(z)}{dz^2} + \sum_{n=1}^L \epsilon_n \delta(z - z_n)\phi(z). \quad (1)$$

Equation (1) defines the Kronig-Penney model where E is the eigenenergy of the stationary states, ϵ_n is the strength of the potential and z denotes space while we take the positions of the δ functions to be regularly spaced ($z_n = n$). The tight-binding model corresponding to Eq. (1) is [11]

$$\phi_{n+1} + \phi_{n-1} = v_n \phi_n, \quad v_n = 2\cos(q) + \epsilon_n \frac{\sin(q)}{q} \quad (2)$$

with $q^2 \equiv E$, $\phi_n \equiv \phi(z = n)$; Eq. (2) can be written equivalently as a two-dimensional map M_n , i.e.:

$$\begin{pmatrix} x_{n+1} \\ y_{n+1} \end{pmatrix} = \begin{pmatrix} v_n & -1 \\ 1 & 0 \end{pmatrix} \begin{pmatrix} x_n \\ y_n \end{pmatrix}, \quad (3)$$

where $\phi_n = x_n$ and $y_n = \phi_{n-1}$. An eigenstate of Eq. (2) is a 'trajectory' of the map of Eq. (3). Straightforward diagonalization of this map leads to the eigenvalues $\lambda_n^\pm = \frac{v_n \pm i\sqrt{4-v_n^2}}{2} = e^{\pm i\mu_n}$ where the phase μ_n is introduced by the relation $v_n = 2\cos\mu_n$. For $|v_n| < 2$ we obtain stable map rotation with phase μ_n . For $|v_n| = 2$ we find the curves separating regions of allowed and forbidden energies, determined through equations $q = (2k+1)\pi$, for $\epsilon = -2q\cot(q/2)$ and $q = 2k\pi$, for $\epsilon = 2q\tan(q/2)$ with $k = 0, 1, 2, \dots$. To understand the origin of the resonant states in the RDKP model resulting when adjacent pairs of random energies ϵ_n coincide [10], we consider the sequence ϵ_n which consists of one dimer only i.e. where all the values of ϵ_n are equal to ϵ_1 except two values for which we have $\epsilon_m = \epsilon_{m+1} = \epsilon_2$. From the property of the map eigenvalues found previously we observe that this unique dimer with energy ϵ_2 does not influence the trajectories of the map of Eq. (3) when the total phase advance $\mu_m + \mu_{m+1} = 2\mu_m$ through the dimer is equal to π or 2π . Since the latter value $\mu_m = \pi$ is forbidden from the stability conditions, the resonant energy $q_{cr}^2 \equiv E_{cr}$ is defined by $\mu_m = \pi/2$ giving $-2q_{cr}/\epsilon_2 = \tan(q_{cr})$. As a result, for the general case of randomly distributed dimers ϵ_1 and ϵ_2 , there are two resonant values,

$$q_{cr} = -\frac{\epsilon_{1,2}\tan(q_{cr})}{2} \quad (4)$$

for which dimers of the first type, ϵ_1 , or of the second, ϵ_2 , have no influence on the transparent states. One should note that since $\tan(q_{cr})$ is a π -periodic function and takes values in $(-\infty, +\infty)$, we have an infinite set of critical energies q_{cr} (two in every interval

$[(2k - 1)\pi/2, (2k + 1)\pi/2]$ [10]. However, for the first allowed band defined through the condition $|v_n| = 2$, the disorder strength ϵ must be greater than a critical value $\epsilon_{cr} = -2$ in order to have resonant states. The critical disorder for reflectionless modes to appear, arises only in the first band of the spectrum.

The previous analysis can be extended to the general case of N -mer (two values ϵ_1 and ϵ_2 appear in blocks of length N) where the resonant energy is defined through the following condition

$$\mu_N = \frac{\pi}{N}, \frac{2\pi}{N}, \frac{3\pi}{N}, \frac{4\pi}{N}, \dots, \frac{(j+1)\pi}{N}; \quad j = 0, 1, 2, \dots, N-2. \quad (5)$$

We note that as the block size N increases the number of resonant states proportional to $2(N-1)$ increases as well. In the first zone, in particular, the disorder strength should be smaller than a critical strength $\epsilon_{cr}(N)$ for this to happen. The latter is obtained through equation $2\cos(q_{cr}) + \epsilon_{1,2} \frac{\sin(q_{cr})}{q_{cr}} = 2\cos\mu_N$ that gives the corresponding critical wavevectors. Equivalently, ϵ_{cr} is obtained through:

$$\frac{\sin q}{\cos q - \cos\mu_N} = -\frac{2q}{\epsilon_{cr}}. \quad (6)$$

The resonances inside the first band appear whenever the derivative of the left hand side of Eq.(6) at $q = 0$ is less than $-\frac{2}{\epsilon_{cr}}$ and thus

$$\epsilon_{cr}(N) = 2(\cos(\mu_N) - 1) \quad (7)$$

In the phase diagram of Fig. 1 we distinguish three regions: (I) contains no resonant states, (II) where some resonant states appear and (III) where all resonants are concentrated. The borders of region (II) start at $\epsilon = -2$ for $N = -2$ (RDKP case) and are given by the curve Eq. (7) with $\mu_N = \pi/N$ (upper bound) and $\mu_N = (N-1)\pi/N$ (lower bound) and approach zero and -4 respectively as $N \rightarrow \infty$. We recall that for the perfect Kronig-Penney lattice the range of accessible ϵ values within the first energy band is $[-4, +\infty)$. We further note that the lower border corresponds to the existence of only one resonant state, while as we are going towards the upper border more resonances appear. The upper critical curve delimits region III in which all system resonances are found.

By introducing a new variable $p_{n+1} = x_{n+1} - x_n$ playing a role similar to momentum we obtain through Eq. (3) a new map representation:

$$\begin{aligned} p_{n+1} &= p_n + f_n x_n \\ x_{n+1} &= x_n + p_{n+1} \end{aligned} \quad (8)$$

where $f_n = v_n - 2$ and having the same eigenvalues with the original map (3). In the map of Eq. (8) ellipses correspond to $\epsilon_n = \epsilon_1$ for all n , a defect at site m with $\epsilon_m = \epsilon_2$ results in a kick into another ellipse (Fig. 2a) while correlated defects lead to a return to the original ellipse, since the total phase advance $\mu = \mu_m + \mu_{m+1} = \pi$ (Fig. 2b). When a random mixture of dimers with energy ϵ_2 is embedded in a chain with energy ϵ_1 , we obtain a phase space trajectory similar to the one in Fig. 2c. We observe two ellipses corresponding to ϵ_1 and ϵ_2 values respectively. The second ellipse is formed by points occurring every time the first site of a dimer is encountered by the map. In the general case of correlated M -block under the condition that the total sum $\sum_{n=1}^M \mu_n$ of phase shifts is equal to $m\pi$, for any sequence with m integer, the trajectory always returns to the ellipse associated with the "perfect" sites to the left and to the right of the scattering potential.

2.2 Parametric Linear Oscillator

Another useful representation of the original model of Eq. (2) similar to the map of Eq. (8) but more convenient for the analysis of the localization length, can be obtained through two successive maps [9]:

$$\begin{aligned} \tilde{p}_n &= p_n + A_n x_n \\ \tilde{x}_n &= x_n \end{aligned} \quad (9)$$

and

$$\begin{aligned} p_{n+1} &= \tilde{p}_n \cos \mu_0 - \tilde{x}_n \sin \mu_0 \\ x_{n+1} &= \tilde{p}_n \sin \mu_0 + \tilde{x}_n \cos \mu_0 \end{aligned} \quad (10)$$

When the maps of Eq. (9) and Eq. (10) are combined, they result in a form of Eq. (2), viz.

$$x_{n+1} + x_{n-1} = (2 \cos \mu_0 + A_n \sin \mu_0) x_n. \quad (11)$$

Comparing with Eq. (2) one can establish the correspondence $\mu_0 = q$; $A_n = \frac{\epsilon_n}{q}$ between the parameters q, ϵ_n in the original model (2) and the parameters μ_0, A_n of the

map of Eq. (9,10). The latter map has a clear meaning since the map of Eq. (9) corresponds to an instant linear kick of the strength A_n resulting in the change of the momentum p_n and the map of Eq. (10) describes free rotation in the phase plane (p, x) defined by the angle μ_0 . The dynamical system modeled by Eqs. (9),(10) is that of a linear oscillator with a periodic parametrical perturbation with a Hamiltonian [9]

$$\tilde{H} = \frac{\mu_0 p^2}{2} + \frac{\mu_0 x^2}{2} - \frac{1}{2} x^2 \tilde{\delta}_1(t); \quad \tilde{\delta}_1(t) \equiv \sum_{n=-\infty}^{\infty} A_n \delta(t - n) \quad (12)$$

We note that by integrating Eq. (1) between two successive δ -kicks of the potential, we obtain Eq. (10), while integration over a kick, results in Eq. (9) with a new kick strength $A_n = \epsilon_n$. By comparing Eq. (1) and Eqs (9),(10) we find the significance of the variable p_n : it is the rescaled (with respect to $q = \sqrt{E}$) first derivative of the local amplitude function ϕ just before the n -th kick i.e. $p_n = (d\phi/dz)_{z=z_n}/q$.

For the dimer case defined by the two values of ϵ_1, ϵ_2 , we can set without loss of generality $\epsilon_1 = 0$. As a result, the motion corresponding to $\epsilon_n = \epsilon_1$ is represented by the circle in the phase plane (p, x) and resonant behavior results when, after a given number of kicks with $\epsilon_n = \epsilon_2$, the trajectory returns to this circle. An example of this behaviour is given in Fig. 3a for $q = q_{cr} = 11.4$ and $\epsilon_2 = 9.75885$. A similar behaviour for the case of a trimer $N = 3$ is illustrated in Fig. 3b for $\epsilon_2 = 1.25$ and $q = q_{cr} = 1.489$. We observe that the trajectory is bounded in the phase-space.

The above scheme is also valid for the much more general case where the locations of the δ - functions z_n in the original model Eq. (1) are not equidistant and can be taken from an arbitrary distribution. In this case Eq. (10) has the same form provided we make the substitution $\mu_0 \rightarrow \mu_{T_n} = qT_n$, where T_n corresponds to random periods of the kicks in the Hamiltonian approach (12). In the original model of Eq. (1), T_n indicates the random distance between two successive lattice sites, i.e. $T_n = z_{n+1} - z_n$. The critical value q_{cr} for the dimer is obtained directly from Eq. (11) using the relation $2 \cos \mu_N = 2 \cos \mu_{T_n} + A_n \sin \mu_{T_n}$ with $\mu_N = \pi/2$ (see Eq. (5)). As a result, we obtain $\tan(q_{cr}T_n) = -\epsilon/(2q_{cr})$ where both T_n and ϵ_n are related to the same lattice site z_n in Eq. (1). Therefore, we conclude that in the case of a generalized dimer where time displacements T_n and on-site

potential are paired, in a way such that $T_n = T_{n+1} = T_2$ and $\epsilon_n = \epsilon_{n+1} = \epsilon_2$, the condition for the critical energy will be similar to the one obtained previously but with the change $\mu_0 \rightarrow \mu_{T_n} = \mu_2 = qT_2$.

2.3 Nearly Resonant States

The representation of the model of Eq. (2) used in section 2.2 allows for the study of global properties of eigenstates. In particular, the resonant delocalized states correspond to a bounded motion described by the maps of Eqs (8),(9),(10). Localized states on the other hand are represented by unbounded trajectories that escape from the origin of phase space (p, x) . This is illustrated in Fig. (4) for the case of random dimers with non-resonant values of q . The exponential increase of a distance from the origin ($p = x = 0$) is related to the localization length of the corresponding eigenstate. In order to study the dependence of the localization length l for nearly-resonant states, it is useful to pass to action-angle variables (r, θ) for the map of Eq. ((9, (10) using the definitions $x = r \cos \theta$ and $p = r \sin \theta$. We obtain a map for the action r given by

$$r_{n+1}^2 = r_n^2 D_n^2; \quad D_n^2 = (1 + A_n^2 \cos^2 \theta_n + A_n \sin 2\theta_n) \quad (13)$$

where the transformation for $\cos \theta_n$ and $\sin \theta_n$ is given by the relations

$$\begin{aligned} \cos \theta_{n+1} &= D_n^{-1} \{ \cos(\theta_n + \mu_0) - A_n \cos \theta_n \sin \mu_0 \} \\ \sin \theta_{n+1} &= D_n^{-1} \{ \sin(\theta_n + \mu_0) + A_n \cos \theta_n \cos \mu_0 \} \end{aligned} \quad (14)$$

The relations of Eq. (13,14) can be used instead of the common transfer matrix approach for the determination of the localization length l . The latter is equal to the inverse of the Lyapunov exponent γ defined as

$$\gamma = \lim_{N \rightarrow \infty} \frac{1}{N} \sum_{n=0}^{N-1} \ln \left(\frac{r_{n+1}}{r_n} \right) \quad (15)$$

where the ratio $r_{n+1}/r_n = D_n$ is given by (13).

The advantage of this approach in the finding of the Lyapunov exponent γ in comparison to the standard transfer matrix method is that there is no divergence during iterations. It is interesting to note that Eqs. (13), (14) can be mapped into a one-dimensional map

$\theta_{n+1} = F(\theta_n)$ which is non-linear for the non-zero perturbation $A_n \neq 0$. One can show that in such a representation, the expression (13) is directly related to the stretching of the phase, $d\theta_{n+1}/d\theta_n = D_n^2$. Therefore, the original quantum problem is reduced to the study of the properties of a one-dimensional time-dependent map and its tangent space.

Due to correlations in the sequence θ_n , the expression (15) can not be evaluated directly. However, it is possible to construct an effective map for two successive kicks of the single map (13) and neglect the correlations between the phases θ_{n+2} and θ_n near the resonance $q = q_{cr} - \delta \approx q_{cr}$. Applying the resulting two-step map [9] to the present case allows us to estimate the Lyapunov exponent for $\delta \ll 1$, using the expansion in $W = A_n\delta/\sin\mu_0$, with the successive averaging over θ_n , leading to

$$\gamma \approx Q \frac{\delta^2 \epsilon_2^2}{\mu_0^2 \sin^2 \mu_0} \quad (16)$$

The factor Q stands for the probability for the dimer of the second kind (with energy ϵ_2), to appear. In Fig. 5 we compare the analytical result (16) (solid line) with the numerical data obtained from the map (13,14) (circles) after iterating up to 4000000 time steps and averaging over more than 1000 realizations of the random kick strengths A_n , for the case $Q = 0.5$, $\epsilon = 9.75885$ and $q_{cr} = 11.4$. The agreement between theory and numerical data is extremely good as seen in Fig. 5 verifying that expression (16) valid for $\delta \ll 1$.

From Eq. (16) we determine the dependence of the inverse of the localization length for the near-resonant states and the way it changes when the system parameters change. We note that the higher the order of the resonance, $q \gg 1$ (i.e. the higher k in $[(2k - 1)\pi/2, (2k + 1)\pi/2]$), the larger is the localization length, and thus better transport properties are expected. Such a behaviour of $l(q)$ is expected since for $q \gg 1$ the second term of v_n (where q appears in the denominator) in Eq. (2) becomes negligible resulting to a tight-binding equation with zero on-site potential. The localization length increases also when decreasing ϵ towards zero. This is easily comprehended since when $\epsilon_1 = \epsilon_2 = 0$ we recover the properties of the perfect lattice. Finally, as the concentration Q of dimers decreases, the value of the localization length for the near resonant states increases.

3 Transport Properties.

In this section we examine the transport properties of our system by studying the behavior of the transmission coefficient. We assume that the system of Eq. (2) is a sample consisting of L lattice points with two identical semi-infinite perfect leads on either side. As a result, the left lead extends from $-\infty < n \leq 0$, the sample extends from $1 \leq n \leq L$ and the right lead extends from $L + 1 < n < \infty$. The purpose of these leads is to carry the incoming, the reflected and the transmitted waves. Here E (see Eq.(1)) is the Fermi energy and without any loss of generality we choose $\epsilon_n = 0$ everywhere in the leads.

In order to calculate the transmission amplitude t_L of a segment containing L sites we inject a particle from $-\infty$ with an energy $\tilde{E} = 2\cos q$ towards the sample. While the particle passes through the sample it undergoes multiple elastic scattering. Eventually, it comes out of the sample from the right end with amplitude t_L . Following Pichard [12] we write the transmission coefficient $T_L = |t_L|^2$ in terms of the matrix elements of the total transfer matrix $P_L = \prod_{n=1}^L M_n$ as

$$T_L = \frac{4|\sin q|^2}{|(P_L)_{21} - (P_L)_{12} + (P_L)_{22}e^{iq} - (P_L)_{11}e^{-iq}|^2}. \quad (17)$$

In the Hamiltonian map approach, the above system corresponds to the parametric linear oscillator of section 2.2 where the strength A_n of the instant linear kick (see Eq. (9)) is equal to zero for times $t \leq 0$ or $t \geq L + 1$ describing free rotations in phase plane, while in the time interval $1 \leq t \leq L$ the strength A_n is determined by the disordered site energy ϵ_n of the underlying one-dimensional Schrödinger equation (1).

In order to establish a relation for the transmission coefficient in the frame of our Hamiltonian map approach, we recast the two successive maps of Eqs (9),(10) to the following two-dimensional map Q_n

$$\begin{pmatrix} x_{n+1} \\ p_{n+1} \end{pmatrix} = \begin{pmatrix} \cos\mu_0 + A_n \sin\mu_0 & \sin\mu_0 \\ A_n \cos\mu_0 - \sin\mu_0 & \cos\mu_0 \end{pmatrix} \begin{pmatrix} x_n \\ p_n \end{pmatrix}, \quad (18)$$

which is related to the transfer matrix M_n defined in Eq. (3) through a similarity transfor-

mation R

$$Q_n = RM_nR^{-1}; \quad R = \begin{pmatrix} 1 & 0 \\ \frac{\cos\mu_0}{\sin\mu_0} & -\frac{1}{\sin\mu_0} \end{pmatrix} \quad (19)$$

From the above Eq.(19) and Eq.(17), one obtains for the transmission coefficient T_L of a system with L scatterers:

$$T_L = \frac{4}{((F_L)_{11}^2 + (F_L)_{21}^2) + ((F_L)_{12}^2 + (F_L)_{22}^2) + 2} \quad (20)$$

where the matrix F_L is the product transfer matrix i.e $F_L = \prod_{n=1}^L Q_n$. From Eq.(20) we see that the sum inside the first parenthesis in the denominator is equal to the inner product of the vector $v(t = L) = F_L \begin{pmatrix} 1 \\ 0 \end{pmatrix}$ i.e. to the modulus square of the vector $v(0) = \begin{pmatrix} 1 \\ 0 \end{pmatrix}$ evolved under the dynamical map (18) (or equivalently under the map (9, 10)) for time $t = L$, in the phase space of the parametric linear oscillator described by the Hamiltonian (12). Similarly, the sum inside the second parenthesis in the denominator in Eq.(20) corresponds to the modulus square after the evolution for time $t = L$ of the initial vector $u(0) = \begin{pmatrix} 0 \\ 1 \end{pmatrix}$. It is interesting to note that the initial vectors $v(0), u(0)$ correspond to the unit vectors pointing to the two perpendicular directions on the phase-space plain.

Using these observations, we can give a geometrical interpretation for Eq.(20) viz. to relate T_L with areas in the phase-space of the two dimensional Hamiltonian map (12). In particular, we can interpret the sum inside each parenthesis in the denominator, as the area of a circle described by a radius r_1, r_2 which is given by the time evolution (under the map (18)) of the initial vectors $(r_{1,2}, \theta_{1,2})_{t=0} = (1, 0), (1, \pi/2)$. Thus Eq.(20) can be rewritten in the following form

$$T_L = \frac{4\pi}{\pi r_1^2 + \pi r_2^2 + 2\pi} = \frac{2S_{tot}^0}{S_{tot}^0 + S_{tot}^L} \quad (21)$$

where $S_{tot}^L = S_1^L + S_2^L$ is the sum of the areas defined by the radius r_1, r_2 at time $t = L$. In the case of perfect lattice where we have simple rotations of the initial vectors $(r_{1,2}, \theta_{1,2})^0$, the areas defined after time L will be the same $S_{tot}^L = S_{tot}^0 = 2\pi$ and hence $T_L = 1$.

Using Eq. (13) we can write Eq.(21) in a way that it is more tractable for numerical

calculations, i.e.

$$T_L = \frac{4}{\prod_{n=0}^{L-1} (D_n^{(1)})^2 + \prod_{n=0}^{L-1} (D_n^{(2)})^2 + 2} \quad (22)$$

where $D^{i=1,2}$ correspond to initial conditions $(r_i, \theta_i)^0 = (1, 0), (1, \pi/2)$ respectively.

The results we have obtained so far provide an exact, although non-closed, analytical description of any one-dimensional system that can be written in the tight-binding form of Eq.(2). We will now evaluate them for the specific case of RDKP to describe those relevant features of the transmission coefficient that may be the fingerprint of extended states.

In Fig. 6a,b we show numerical results for a system of 10000 scatterers after averaging over more than 10000 different realizations of the disordered sample. We take the values of $\epsilon_1 = 0$ and $\epsilon_2 = 9.75885$ and the defect concentration $Q = 0.5$, i.e. the most random case. In Fig. 6a we used the critical energy $q_{cr} = 5.443223$ lying inside the second zone of the spectrum while Fig. 6b $q_{cr} = 33.13$ lying inside the 10^{th} zone. We note that states close to the resonant energies have very good transmission properties, similar to those at the resonant energy where the transmission coefficient T is equal to one. This is compatible with the findings of the random dimer model with one-band (tight-binding approximation) [8]. Moreover in RDKP model, the width of the peaks depends on the order of the resonance, as mentioned previously (see also [10]). From the comparison between Fig. 6a and Fig. 6b we see that the higher the resonance the wider the band of states with $T \approx 1$. In Fig. 6c we presented results for a different defect concentration Q in order to study the dependence of the transmission coefficient depends on Q . We use the same values of ϵ_1, ϵ_2 and $Q = 0.2$. By comparison with Fig. 6a we conclude that as Q decreases the number of transparent states, i.e states with transmission coefficient close to one $T \sim 1$, increases, in perfect agreement with the results of the previous section for the localization length of nearly-resonant states.

4 Conclusions

We have studied a Kronig-Penney model with binary on-site disorder randomly assigned every two sites. For such a model it was found [10] that there exist infinite number of

special energies $E_{cr} = q_{cr}^2$ at which transparent states appear. We recover these results using a new approach based on classical Hamiltonian maps. We generalized our results for a N -mer case and obtained a simple expression for the resonant energy values. We constructed a phase diagram in the $\epsilon_{cr} - N$ plane which marks three distinct regions: one where no resonant states appear, the second that contains some of the resonant states and the third that contains all possible resonant states for different correlated blocks of size N . This separation in three distinct regions is valid only in the first zone and as a result it might have some relevance to the low temperature system properties. Our dynamical system approach maps resonant delocalized states to bounded trajectories, while localized states are represented by unbounded trajectories in the phase space (p, x) . Making use of an expansion in the vicinity of the resonance, we derived an analytical expression of Eq. (16) for the Lyapunov exponent for the nearly resonant states. Finally, in the frame of our Hamiltonian map we established a simple geometrical picture for the transmission coefficient showing that it corresponds to evolution of areas in the phase space of a linear parametric oscillator. Using these last results we calculated the transmission coefficient that exhibits peaks up to $T = 1$ for energy values equal to the resonant ones. Near the resonant energies there are nearly-transparent states with large transmission coefficient, the number of which is inversely proportional to the defect concentration Q and increases with the resonance order. The properties of the RDKP model that were analyzed in this work could be used to several mesoscopic quasi-one dimensional studies.

4.1 Acknowledgment

We acknowledge support of ΠΕΝΕΔ 95-115 grant of the General Secretariat for Research and Technology of Greece. One of the authors (F. M. I.) wishes to acknowledge support of Grant ERBCHRXCT 930331 Human Capital and Mobility Network of the European Community; and the support of Grant No RB7000 from the International Science Foundation. (T. K.) acknowledges with thanks many useful discussions on the Anderson localization with A. Politi during his visits to the Istituto Nazionale di Ottica.

References

- [1] D. Dunlap, H.-L. Wu and P. Phillips, Phys. Rev. Let. **65**, 88 (1990).
- [2] P. Phillips and H.-L. Wu, Science **252**, 1805 (1991).
- [3] A. Bovier, J. Phys. A **25**, 1021 (1992).
- [4] J. C. Flores, J. Phys. Cond. Matt. **1**, 8471 (1989).
- [5] S. Gangopadhyay and A. K. Sen, J. Phys. Cond. Matt. **4**, 9939 (1992).
- [6] S. N. Evangelou and E. N. Economou, J. Phys. A **26** , 2803 (1993).
- [7] S. N. Evangelou and A. Z. Wang, Phys. Rev. B **47** , 13126 (1993).
- [8] (a) P. K. Datta, D. Giri and K. Kundu, Phys. Rev. B **47**, 10727 (1993); (b) P. K. Datta, D. Giri and K. Kundu, Phys. Rev. B **48**, 16347 (1993)
- [9] F.M.Izrailev, Tsampikos Kottos and G. P. Tsironis, Phys. Rev. B **52**, 3274 (1995); J. Phys.: Condens. Matter **8**, 2823 (1996).
- [10] Angel Sánchez, Enrique Maciá and Francisco Domínguez-Adame, Phys. Rev. B, **49**, 147 (1994).
- [11] J. Bellissard, A. Formoso, R. Lima and D. Testard, Phys. Rev. B **26**, 3024 (1982).
- [12] J. L. Pichard, J. Phys. C : Solid State Phys. **19**, 1519 (1986).

Figure Captions

Figure 1: The phase diagram showing the critical ϵ_{cr} values as a function of the block size N .

Figure 2: Phase space of the map of Eq. (13) for $p_0 = x_0 = 1$:

(a) One value of ϵ_2 in the sequence $\epsilon : \dots \epsilon_1 \epsilon_1 \epsilon_1 \epsilon_2 \epsilon_1 \epsilon_1 \epsilon_1 \dots$ for $q_{cr} = 11.4$;

$\epsilon_1 = 0$; $\epsilon_2 = 9.75885$; We note that one point is outside of the ellipse representing the kick to the ϵ_1 trajectory by ϵ_2 .

(b) Two values of ϵ_2 (one dimer) in the sequence $\epsilon : \dots \epsilon_1 \epsilon_1 \epsilon_1 \epsilon_2 \epsilon_2 \epsilon_1 \epsilon_1 \epsilon_1 \dots$ for $\epsilon_1 = 0$; $\epsilon_2 = 9.75885$; $q_{cr} = 11.4$. We note that there is a point inside the ellipse representing the kick to the ϵ_1 trajectory by the first ϵ_2 value. The second ϵ_2 value kicks the trajectory back to the ellipse.

(c) Dimers of type ϵ_2 , randomly (with probability $Q = 0.5$) distributed in the sequence ϵ for $\epsilon_1 = 0$, $\epsilon_2 = 9.75885$ and $q_{cr} = 11.4$.

Figure 3: The phase space of the map (16-17) for $p_0 = x_0 = 1$ and $Q = 0.5, \epsilon_1 = 0$:

(a) $N = 2$ (dimer); $q_{cr} = 11.4$; $\epsilon_2 = 9.77885$;

(b) $N = 3$ (trimer); $q_{cr} = 1.489$; $\epsilon_2 = 1.25$;

The length of sequence ϵ is equal to $L = 1000$.

Figure 4: Nearly resonant states for a dimer ($N = 2$). Comparing with the resonant states shown in Figs.2-3a, nearly-resonant states correspond to the unbounded (for $t \rightarrow \infty$) motion with a slow spread of the points in the phase space:

(a) $q = 11.399$; $\epsilon_2 = 9.75885$;

(b) $q = 11.390$; $\epsilon_2 = 9.75885$;

(c) $q = 11.38$; $\epsilon_2 = 9.75885$;

Figure 5: Numerical (circles) and analytical estimation (solid line) of the Lyapunov exp. for near resonant states. We use $q_{cr} = 11.4$. We observe good agreement.

Figure 6: Transmission coefficient (averaged over more than 10000 realizations) as a function of $q = E^2$ for a system with $\epsilon_1 = 0$, $\epsilon_2 = 9.75885$:

(a) $Q = 0.5$ and $q_{cr} = 5.44$ corresponding to a resonance inside the second band.

(b) $Q = 0.5$ and $q_{cr} = 33.13$ corresponding to a resonance inside the 10th energy band.

We note that with respect to (a) the band of states with $T \approx 1$ is wider.

(c) $Q = 0.2$ and $q_{cr} = 5.44$ corresponding to a resonance inside the second energy band. We note that with respect to (a) we have now more states with $T \approx 1$.

Fig.1

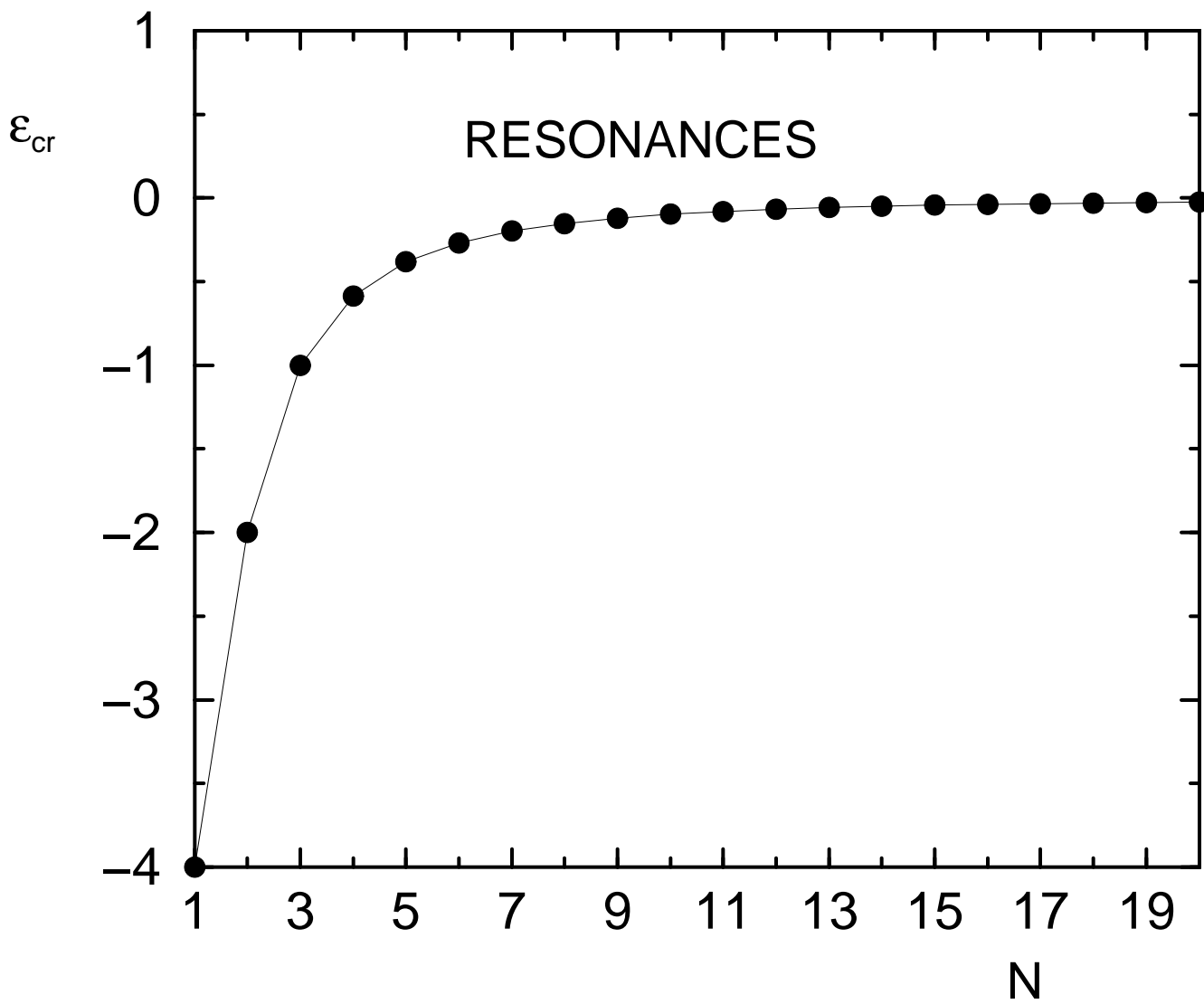


Fig.2a

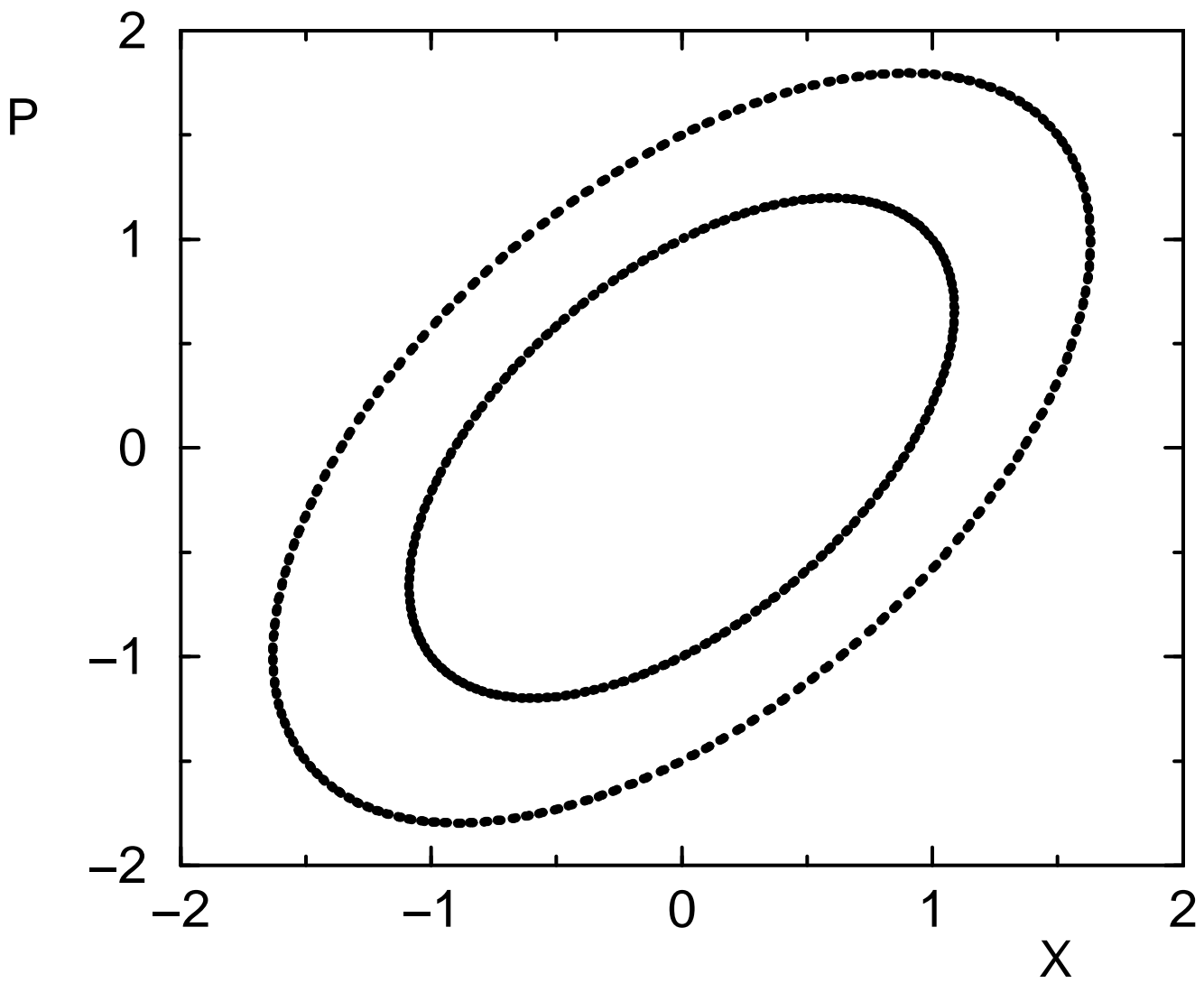


Fig.2b

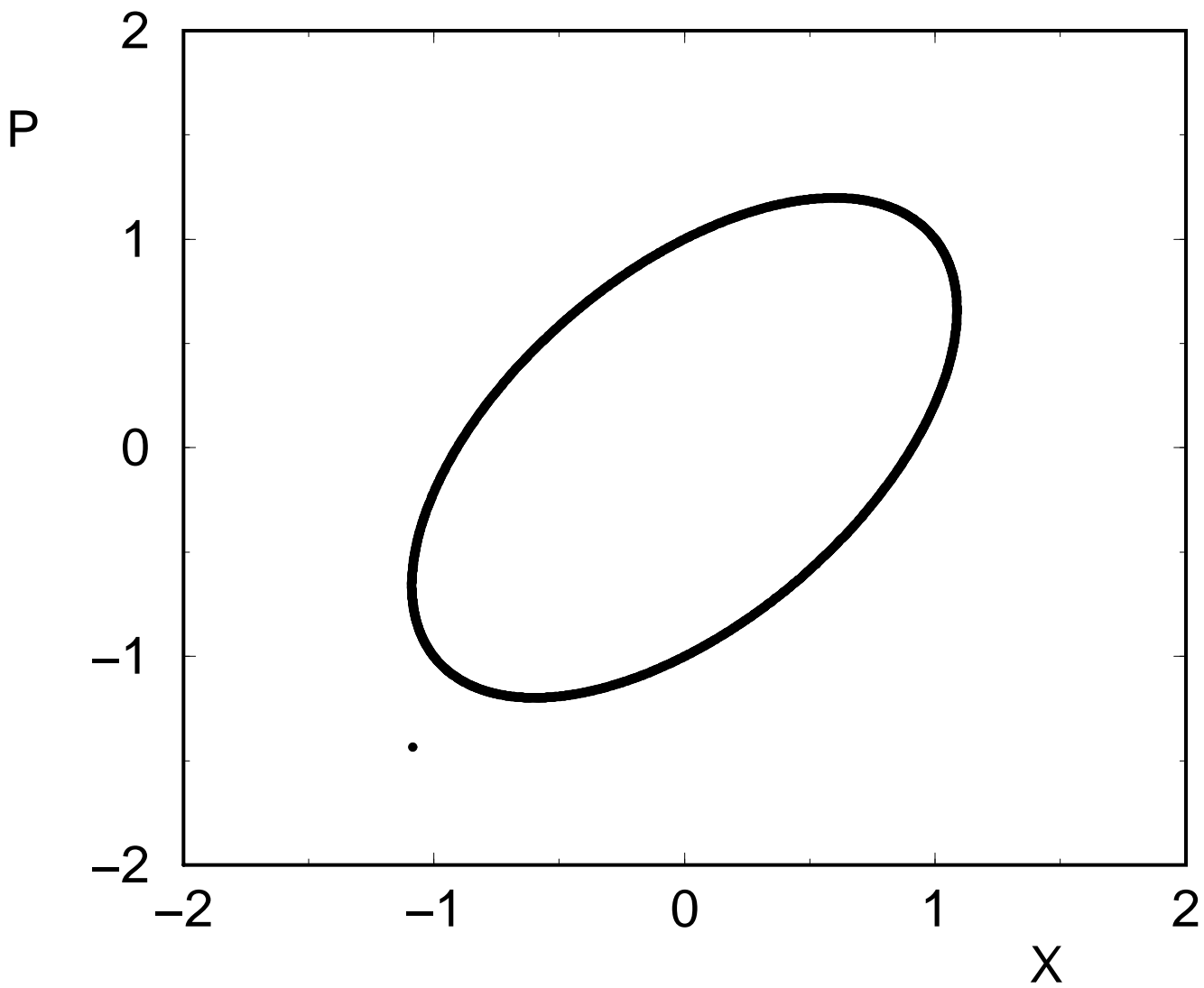


Fig.2c

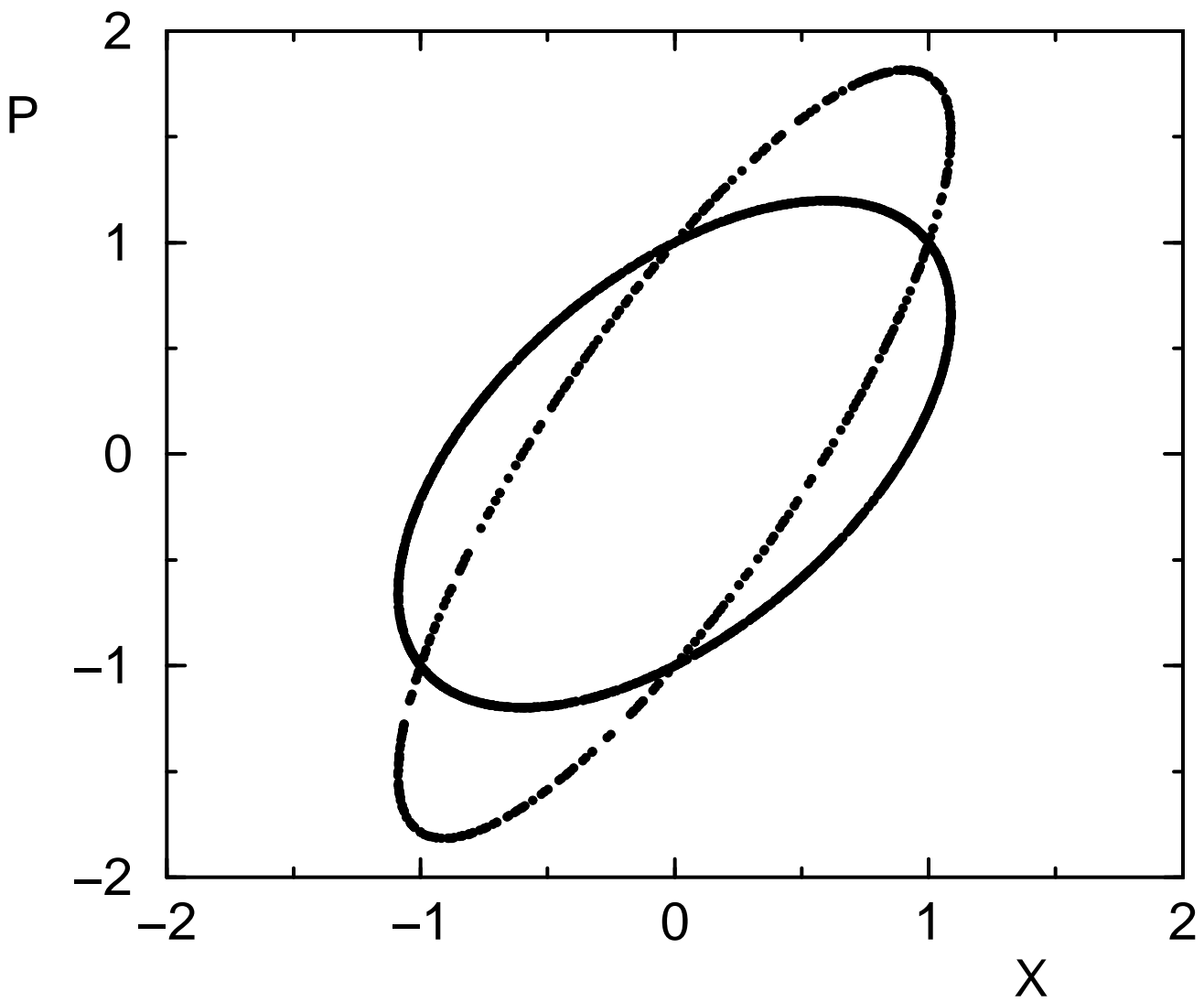


Fig.4a

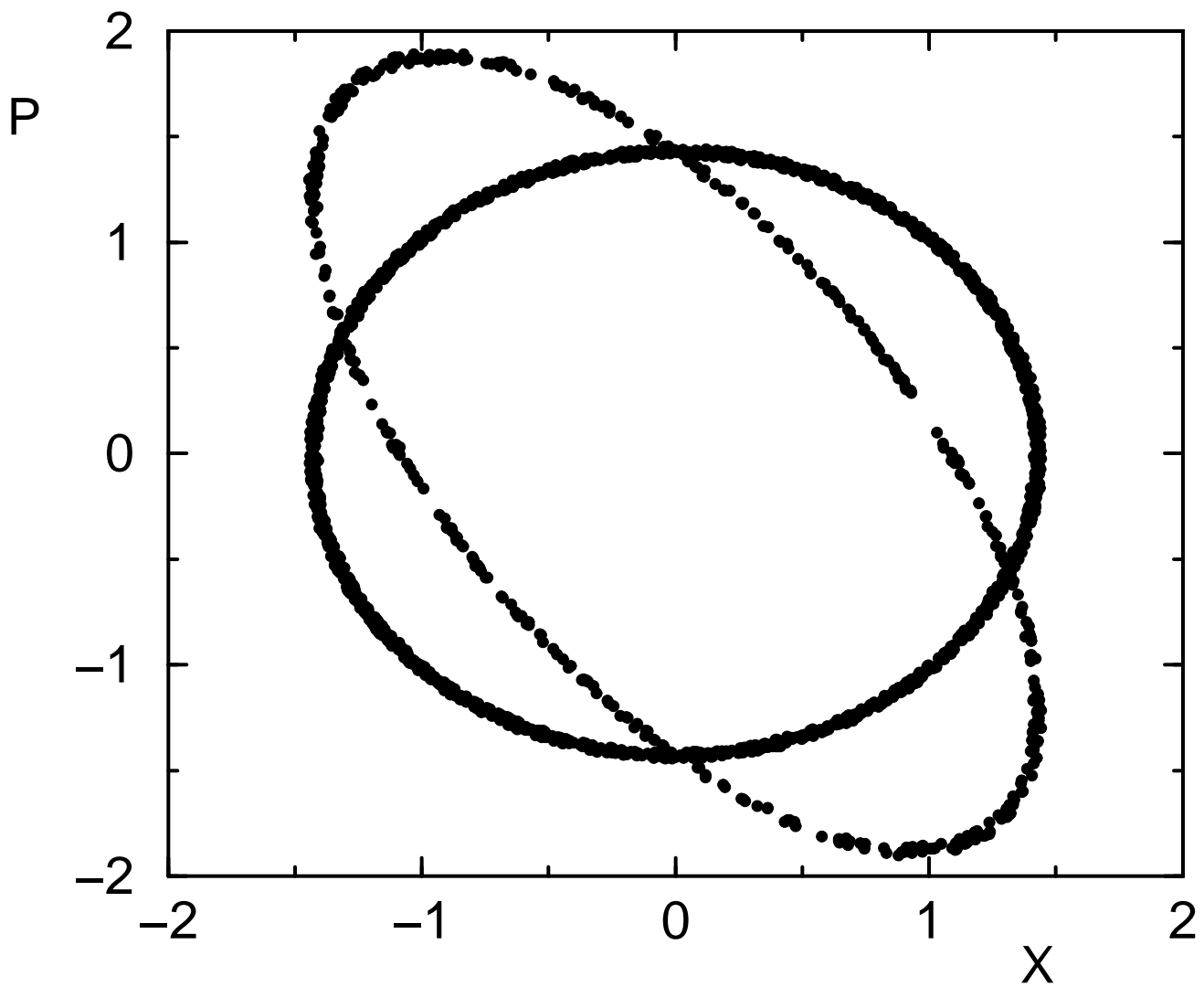


Fig.4b

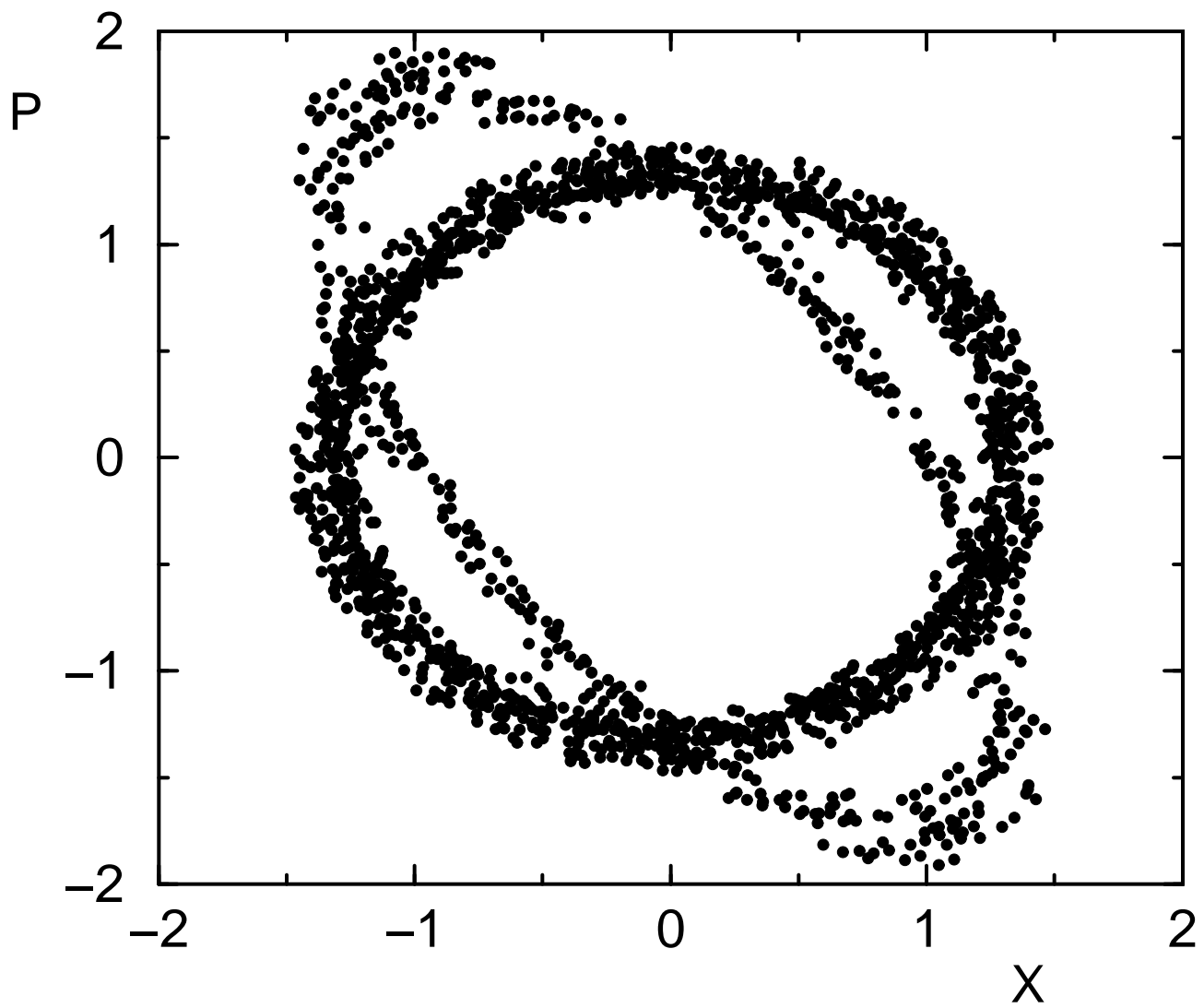


Fig.4c

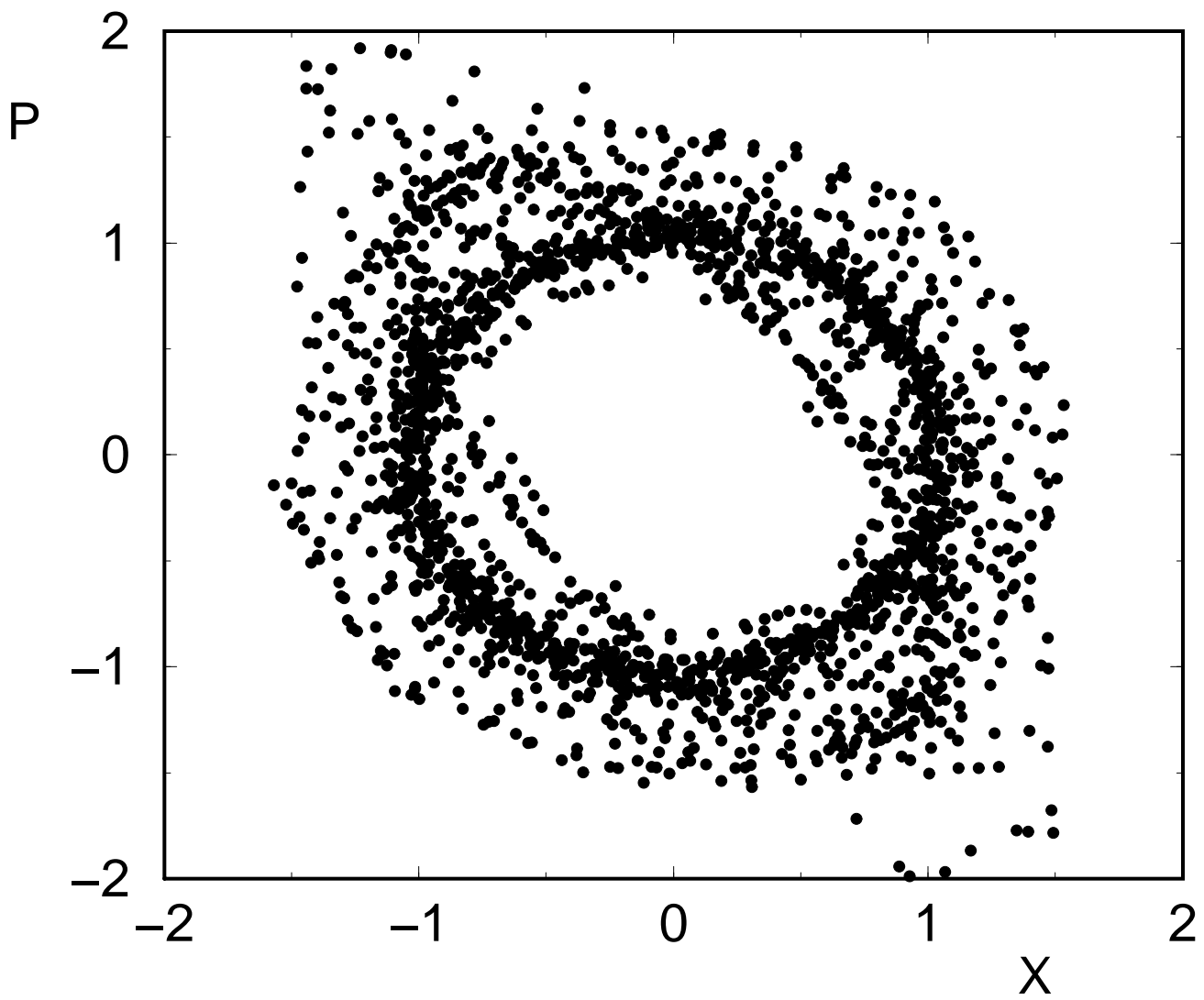


Fig.5

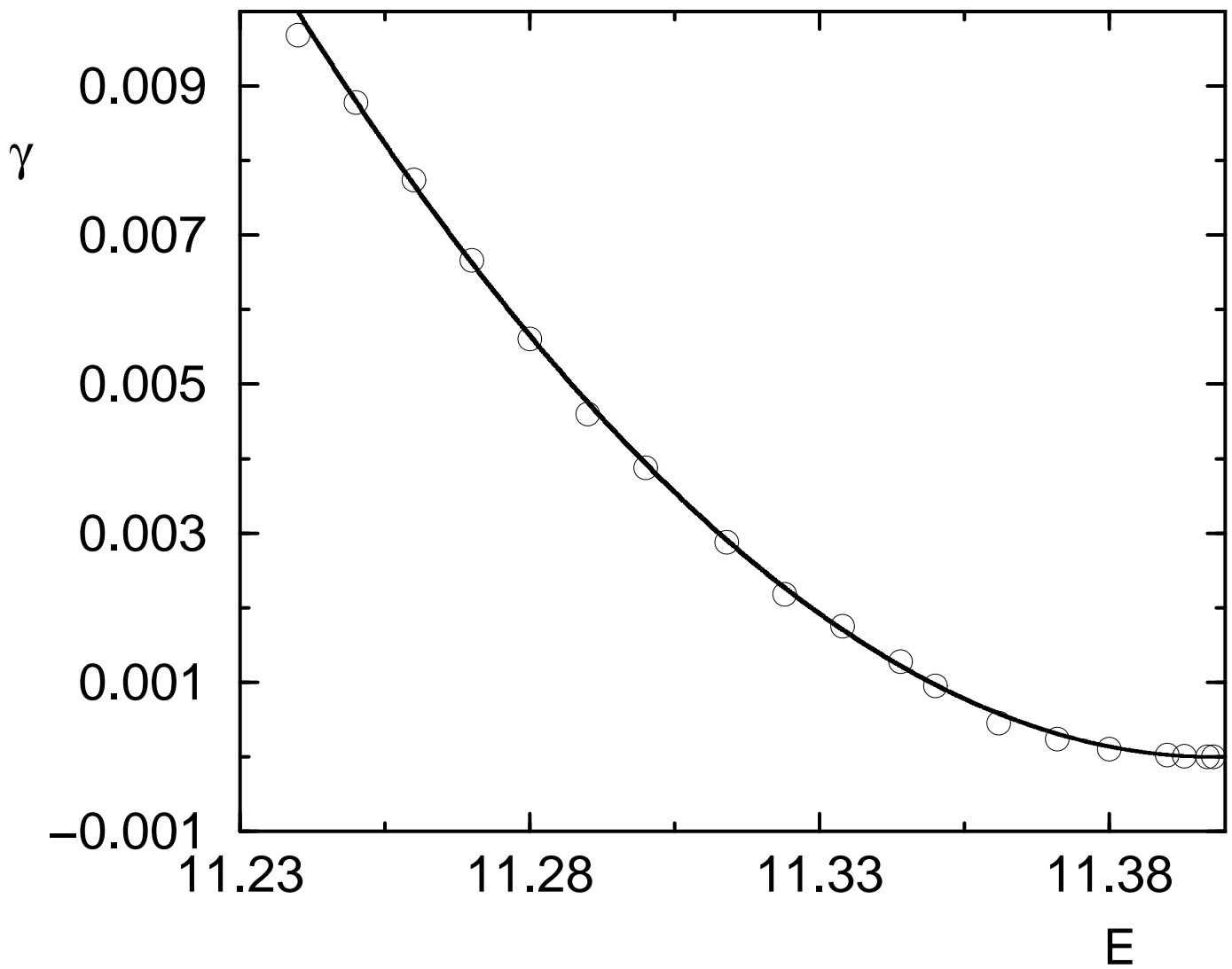


Fig.6a

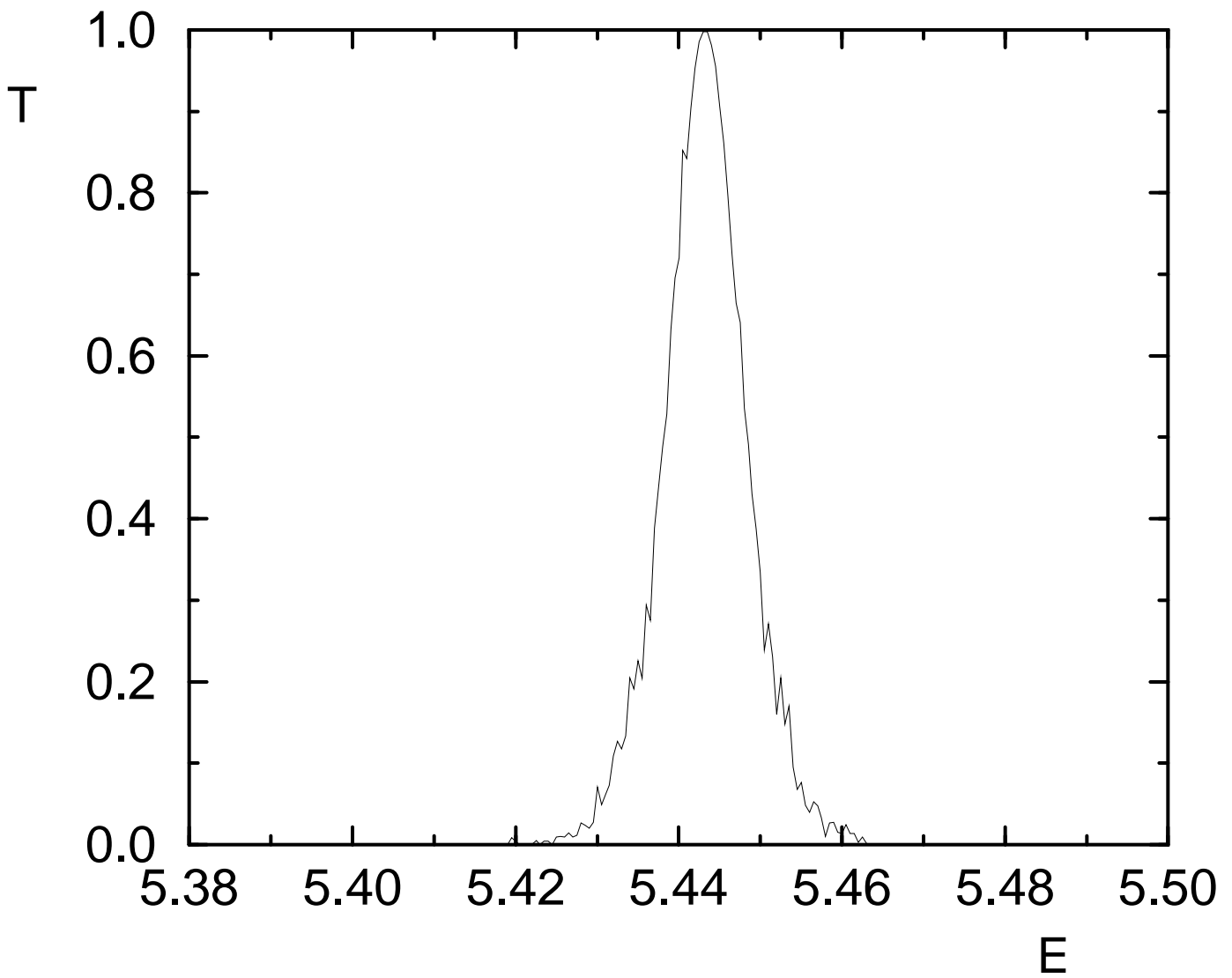


Fig.6b

